

# **TITLE:**

Hit-and-run silencing of endogenous *DUX4* by targeting DNA hypomethylation on D4Z4 repeats in facioscapulohumeral muscular dystrophy

# **AUTHORS:**

Mitsuru Sasaki-Honda<sup>1,\*</sup>, Tatsuya Jonouchi<sup>1</sup>, Meni Arai<sup>1</sup>, Junjie He<sup>1</sup>, Kazusa Okita<sup>2</sup>, Satoko Sakurai<sup>2</sup>, Takuya Yamamoto<sup>3</sup>, Hidetoshi Sakurai<sup>4,\*</sup>

# **AFFILIATIONS:**

<sup>1</sup> Department of Clinical Application, CiRA, Kyoto University, Kyoto 606-8507, Japan.

<sup>2</sup> Department of Life Science Frontiers, CiRA, Kyoto University, Kyoto 606-8507, Japan.

<sup>3</sup> Department of Life Science Frontiers, CiRA, Kyoto University, Kyoto 606-8507, Japan; Institute for the Advanced Study of Human Biology (ASHBi), Kyoto University, Kyoto 606-8501, Japan; Medical Risk Avoidance Based on iPS Cells Team, RIKEN Center for Advanced Intelligence Projects (AIP), Kyoto 606-8507, Japan.

<sup>4</sup> Department of Clinical Application, CiRA, Kyoto University, Kyoto 606-8507, Japan; Takeda-CiRA Joint Program, Fujisawa, Kanagawa 251-8555, Japan.

**\*Corresponding author: Hidetoshi Sakurai, M.D., Ph.D., Center for iPS Cell Research and Application (CiRA), Kyoto University, 53 Shogoin Kawahara-cho, Sakyo-ku, Kyoto 606-8507, Japan. Telephone: 81-75-366-7055; E-Mail: [hsakurai@cira.kyoto-u.ac.jp](mailto:hsakurai@cira.kyoto-u.ac.jp)**

## ABSTRACT

Facioscapulohumeral muscular dystrophy (FSHD), a progressive skeletal muscle disorder, is epigenetically characterized by DNA hypomethylation of the D4Z4 repeats in the 4q35 region, which enables aberrant *DUX4* expression. Sustainable *DUX4* suppression is thus a promising therapeutic strategy by which to prevent disease progression, but most of the supposed methods to achieve this depend on the expression of a mediator biochemical entity that would potentially narrow the quality of life of individuals with FSHD in the clinical context. In this study, we report that by applying hit-and-run silencing with dCas9-mediated epigenetic editing targeting DNA hypomethylation on D4Z4 repeats, we could achieve the suppression of endogenous *DUX4* in our FSHD patient-derived iPSC model. Notably, DNA methylation was significantly upregulated in FSHD cells and suppression effects were observed for at least two weeks after intervention, which was not the case with transient treatments of typical dCas9-KRAB alone. Off-target analysis showed that despite the potential genome-wide risk for DNA methylation, the impact on the transcriptome was limited. We propose that hit-and-run silencing could be a promising option to prevent disease progression with minimum intervention for individuals with FSHD, motivating further study for clinical development.

**Keywords:** facioscapulohumeral muscular dystrophy, progressive skeletal muscle disorder, epigenetics, DNA methylation, *DUX4* suppression, dCas9-mediated epigenetic editing

## INTRODUCTION

Facioscapulohumeral muscular dystrophy (FSHD) is a muscle disorder resulting in progressive muscle weakness and is genetically caused by the contraction of D4Z4 repeats (< 10) in the 4q35 region (FSHD1) or mutations of chromatin regulators such as *SMCHD1*, *DNMT3B*, and *LRIF1* with normal but relatively short D4Z4 repeats (FSHD2)<sup>1-4</sup>. Disease manifestation in both types requires a permissive allele with the shorter D4Z4 repeats cis-combined with haplotype 4qA containing a polyA signal (PAS), leading to stabilized *DUX4* transcription, which is normally silenced in most somatic cells<sup>5-7</sup>. Ectopically expressed *DUX4* can activate a cascade of genes that are not associated to muscle function including early embryonic state-related genes<sup>8</sup> and cause deleterious cellular outcomes<sup>9,10</sup>. Therefore, suppression of *DUX4* transcription or translation is considered a potent therapeutic strategy by which to stop disease progression<sup>11-14</sup>.

While several reports have proposed the administration of chemical compounds aimed at RNA interference<sup>15-18</sup> or blocking signal transduction<sup>19</sup> with promising results to reduce *DUX4* activity, the effects of these strategies always depend on continuous treatment due to chemical instability and may force patients to semi-permanent frequent drug administration. Genome editing, however, provides an option to achieve permanent transcriptional repression, but some reports have shown skeptical results after the removal of PAS on 4qA due to stochastic effects and layered of efficiency issues, including delivery, binding, and rewriting as desired<sup>20,21</sup>. The targeting of the *DUX4* gene body or promoter is still difficult to control as it is located inside a repetitive D4Z4 unit. Moreover, genome editing strategies generally also face technical and ethical issues provoked by the irreversible off-target risks and the creation of

unnatural mutations<sup>22,23</sup>. Beyond the distinct genotypes of FSHD, D4Z4 repeats on the permissive allele are commonly epigenetically characterized with DNA hypomethylation in both FSHD1 and FSHD2, which allows abnormal chromatin relaxation and *DUX4* transcription in muscle cells<sup>24</sup>. Therefore, upregulation of DNA hypomethylation to non-FSHD like hypermethylation in D4Z4 repeats in FSHD cells is a potential therapeutic strategy by which to stably block aberrant *DUX4* transcription and prevent disease progression.

The CRISPR/Cas9 system as a feasible platform for targeted genome editing, opened a path by which to edit the epigenome by creating a catalytically inactive or “dead” Cas9 (dCas9) with sustained sequence-specific targeting capacity<sup>25–27</sup>. Recently various kinds of tools for targeted epigenetic modulation based on dCas9 have been developed to achieve gene expression regulation and are considered to be potential therapeutic methods for pathogenic conditions including congenital diseases<sup>28–30</sup>. Indeed, it was reported that the Krüppel associated box (KRAB) domain fused to dCas9 (dCas9-KRAB) and MeCP2 transcription repression domain (TRD) fused to dCas9 (dCas9-TRD) repressed *DUX4* expression in FSHD patient derived myoblasts and an FSHD mouse model respectively, indicating that targeting *DUX4* by dCas9-based epigenetic repression could be a promising strategy to cure FSHD<sup>31,32</sup>. As the KRAB domain, mainly considered to increase H3K9 tri-methylation via recruitment of KAP1, and MeCP2 TRD, mainly considered to recruit histone deacetylase corepressor complex, may be able to exert limited suppressive effects when expressed<sup>33</sup>, their stable and constitutive expression is supposed to be required for clinical use. However, a recent study showed that the induction of the Cas9 protein provoked immune response in a muscular dystrophy canine model<sup>34</sup>, indicating a potential barrier against Cas9 associated components that are expressed in a constitutive manner

in the context of clinical situations. Moreover, recent clinical trials utilizing AAV vectors, broadly considered as a potent delivery method of transgenes to muscle tissue<sup>35,36</sup>, have led to lethal cases<sup>37,38</sup>, provoking the question of balance between risk and benefit to individuals with FSHD that show relatively mild and gradual disease progression in most cases. This problem could be avoided if an alternative method is developed to sustainably suppress endogenous *DUX4* expression in patient cells by transient induction of dCas9 components that can also be combined with a suitable delivery method.

Among various modifications, DNA methylation is a potent target by which to achieve stably lasting epigenetic effects when compared to histone modifications in terms of epigenetic editing<sup>33,39–41</sup>. Moreover, it was reported that “hit-and-run” co-localized induction of KRAB and DNA methyltransferases associated domains such as DNMT3A catalytic domain can induce lasting silencing effects at a targeted genomic site through the upregulation of local DNA methylation by transient transfection<sup>42</sup>. In addition, the additional co-localization of non-enzymatic DNMT3L can enhance DNA methyltransferase enzymatic activity and “hit-and-run” effects<sup>43–46</sup>. Given that the chromatin state is tightly linked with DNA hypermethylation on D4Z4 repeats in non-FSHD cells in contrast to abnormal relaxation with DNA hypomethylation in FSHD cells, the co-localized combination of these dCas9-mediated suppressive components targeting D4Z4 repeats was considered to suppress endogenous *DUX4* expression in FSHD patient cells. Here, using our patient-derived iPSC model in which patient-specific *DUX4* activity was validated in the context of myogenic differentiation<sup>47</sup>, we provide the proof of concept for the hit-and-run silencing strategy against endogenous *DUX4* gene expression in both FSHD1 and FSHD2, indicating the potential of clinical applications beyond the

96 distinct genetic backgrounds of FSHD.

97

## 98 RESULTS

### 99 Development and validation of dCas9-effector activity

100 First, various potential suppressive effectors fused to dCas9 and sgRNAs targeting D4Z4 repeats were built on a  
 101 piggyBac backbone, which enabled a switch between transient or constitutive expression of components with or  
 102 without simultaneous transfection of PBase (Figure 1A). The effectors included KRAB, catalytic domains of  
 103 DNMT3A (D3A) and DNMT3B (D3B), a pseudo-catalytic domain of DNMT3L (D3L), an enhanced effector  
 104 composed of D3A fused to D3L (D3A3L), and a negative control sequence (Neg). Four sgRNA target sequences  
 105 were selected that have D4Z4 targeting activity, and which were previously validated by Himeda et al with dCas9-  
 106 KRAB<sup>31</sup>. Each dCas9-effector with all the sgRNA vectors were electroporated into an FSHD2 iPS<sup>tet-MyoD</sup> clone, which  
 107 was previously established as FSHD patient-derived iPSC model with *DUX4* and its downstream targets robustly  
 108 expressed after myogenic differentiation<sup>47</sup> (Figure 1B). One week after electroporation, cells were sorted for the dual  
 109 positive population in BFP and RFP, which were cultured for another week to allow then to expand and differentiate  
 110 into myocytes (Figure S1A). *DUX4* and its downstream targets (*ZSCAN4*, *MBD3L2*, and *TRIM43*) were significantly  
 111 suppressed by dCas9-KRAB, which was consistent with a previous report (Figure 1C, 1D). dCas9-D3A, D3L, and  
 112 D3A3L, but not D3B, could suppress *DUX4*, but the effects were not comparable to dCas9-KRAB. Among all the  
 113 conditions, myogenic differentiation was comparable (Figure 1E). DNA methylation analysis showed that  
 114 methylation on the D4Z4 repeats was broadly upregulated by dCas9-KRAB, D3A, and D3A3L and partially  
 115 upregulated by D3L (Figure 1F, S1B). These data confirmed the enzymatic activity of these dCas9 effectors and the  
 116 evaluability of their *DUX4* suppression effect in our FSHD-iPSC model.

117

## 118 **Synergistic effect of dCas9-KRAB and dCas9-D3A/D3A3L**

119 Next, based on the *DUX4* suppression effect and methylation analysis in our results and the limited effects of the  
 120 transient transfection of single effectors previously reported<sup>42</sup>, we evaluated the hit-and-run effect with a combination  
 121 of dCas9-KRAB and dCas9-D3A/D3A3L using transient induction. As dCas9 constructs are too large to be  
 122 introduced into each cell during a single transfection, the system was modified with the dCas9-KRAB construct  
 123 accompanied with a neomycin resistance gene, dCas9-KRAB(Neo), instead of BFP (Figure 2A). This meant that the  
 124 cells were positive for both dCas9-KRAB(Neo) and dCas9-D3A/D3A3L(BFP) when selected based on drug  
 125 resistance against neomycin and by FACS for the BFP signal. First, FSHD2 iPS<sup>tet-MyoD</sup> cells were transfected with  
 126 dCas9-KRAB(Neo) or dCas9-Neg(Neo) with PBase for constitutive expression and maintained with a neomycin  
 127 supplement. (Figure 2B). Then, cells were electroporated with all sgRNAs with dCas9-D3A or dCas9-D3A3L, or  
 128 only sgRNAs. In addition, constitutive KRAB induction (cK) was prepared as positive control of *DUX4* (Figure 2C).  
 129 Two days after sgRNAs and dCas9-D3A/D3A3L(BFP) transfection, cells were sorted for dual RFP+BFP+ positive  
 130 cells, and following two weeks of cell expansion, 10 days of myogenic differentiation was conducted (Figure 2B,  
 131 S2A). Gene expression analysis showed that the transient activity of dCas9-KRAB did not suppress *DUX4*, while the  
 132 transient combination of dCas9-KRAB and dCas9-D3A or dCas9-D3A3L slightly suppressed *DUX4* and its targets  
 133 but was not comparable to cK (Figure 2D, 2E). Among all the conditions, myogenic differentiation was not  
 134 significantly affected, which indicated that the observed slight suppression of *DUX4* in the condition with the  
 135 combination was not due to disrupted muscle differentiation but to the activity of the dCas9-effectors (Figure 2F).



These data indicated that the combined activity of dCas9-KRAB and dCas9-D3A/-D3A3L could slightly suppress *DUX4* even after two weeks of expansion and 10 days of myogenic differentiation unlike dCas9-KRAB alone.

### **Repeated treatment enhanced the suppression effect in the FSHD2 model**

A slight but significant effect at least on *DUX4* targets was observed by transient activity of the combination (Figure 2E), we hypothesized that repeated transfection might enhance the effect. Therefore, dCas9-KRAB(Neo) cells were transfected with sgRNAs and dCas9-D3A3L with 7 day intervals, and up to three times (Figure 3A, 3B). Cells were sorted for dual positive populations with RFP and BFP signals two days after each transfection (Figure S3A, S3B, S3C). FACS data analysis confirmed that most of the cells were not positive for BFP nor RFP one week after electroporation (Supplementary figure 3D). Two weeks after the final transfection, cells were then differentiated into muscle cells. While dCas9-Neg(Neo) cells and dCas9-KRAB(Neo) cells with transient sgRNAs transfection showed comparable *DUX4* expression, dCas9-KRAB(Neo) cells with one, two, and three rounds of sgRNAs and dCas9-D3A3L together (tEP1, tEP2 and tEP3) showed gradual levels of *DUX4* suppression without affecting myogenic differentiation (Figure 3C, 3D, 3E). Notably, suppression of *DUX4* and its target genes in the cells with three rounds was comparable to that in the cK which constitutively induce dCas9-KRAB and sgRNAs expression (Figure 3C, 3D). Transcriptome analysis for two independent sets of transfection experiments confirmed broad suppression of *DUX4* target genes and unaffected muscle differentiation in tEP3 cells (Figure 3F, 3G, 3H). Moreover, DNA methylation analysis on the D4Z4 repeats showed that the methylation was dramatically upregulated over a whole analyzed region in tEP3 cells when compared to the original FSHD2 iPS<sup>tet-MyoD</sup> cells, which showed DNA hypomethylation in contrast

to non-FSHD derived cells, and was consistent with previous clinical genetic studies<sup>48</sup> (Figure 3I, S3E). These data supported the concept that the repeated induction of combined activity of dCas9-KRAB and dCas9-D3A3L could establish sustainable *DUX4* suppression in FSHD2 cells through robust upregulation of DNA methylation on the D4Z4 region.

#### **Hit-and-run silencing could also suppress *DUX4* in the FSHD1 model**

Next we investigated whether the same hit-and-run strategy could be applied in FSHD1 beyond genetic differences as FSHD1 cells have abnormally fewer D4Z4 repeats than the FSHD2 cells or non-FSHD cells. As our FSHD1 clone has low efficiency in electroporation, the protocol was modified where cells were firstly transfected with dCas9-KRAB(Neo) or dCas9-Neg(Neo), dCas9-D3A3L(BFP) or dCas9-Neg(BFP), and PBase together, followed by neomycin selection and sorting for BFP (Figure 4A, 4B). Then these dual dCas9 cells were transfected with sgRNAs three times, sorted for RFP and BFP two days after each transfection, expanded for two weeks after the third transfection, and differentiated into myocytes. FSHD2 cells, treated with this method, showed signatures of *DUX4* gene suppression and upregulation of DNA methylation on the D4Z4 region, consistent with the previous results, and thus validating the method (Figure S4A-H). Fluorescence signals of RFP showed that transfected sgRNAs plasmids did not remain one week after the third transfection (Figure 4C, S4C). Importantly, FSHD1 cells, treated with this method, also showed the signature of *DUX4* suppression, while transient activity of dCas9-KRAB could not suppress *DUX4* (Figure 4D, 4E, 4F). Cells were also prepared with the transfection of both sgRNAs and PBase as constitutive dCas9-KRAB(Neo) active controls and showed *DUX4* suppression, indicating that the extent of the *DUX4*

suppression was comparable between constitutive dCas9-KRAB activity and the transient combination of dCas9-KRAB and dCas9-D3A3L(Figure 4B, 4D, 4E). These data supported the concept that the transient induction of the combined activity of dCas9-KRAB and dCas9-D3A3L targeting D4Z4 can suppress *DUX4* gene expression in both FSHD1 and FSHD2 cells.

### **Minimum off-target impacts on gene expression despite the global effect on DNA methylation**

Next we investigated the genome-wide off-target effects of our hit-and-run strategy by utilizing Infinium Methylation EPIC array. To estimate the maximum off-target effects of the enzymatic activity to cover potential sensitive sites, global DNA methylation was compared among the conditions as follows: 1) tNN (from Figure S4G-H); FSHD2 iPS<sup>tet-MyoD</sup> cells with dCas9-Neg(Neo) and dCas9-Neg(BFP) constitutively introduced and sgRNAs transiently transfected three times; 2) tKD (from Figure S4G-H); FSHD2 iPS<sup>tet-MyoD</sup> cells with dCas9-KRAB(Neo) and dCas9-D3A3L(BFP) constitutively introduced and sgRNAs transiently transfected three times (Figure 5A). PCA analysis showed clear segregation among sample types, confirming the quality of the normalized data (Figure S5A). A biased tendency to upregulation in tKD indicated major potential enzymatic off-target effects for DNA methylation with constitutive expression of KRAB and D3A3L, consistent with previous reports<sup>44</sup> (Figure 5B, S5B, S5C). The differentially upregulated probes were annotated to relevant genes (Figure 5C, 5D, S5D) and merged on RNA-seq data in differentiated myocytes in Figure 3 to predict the potential off-target effects on gene expression (Figure 5C, 5E). Only two genes (*SCL34A2* and *CCNA1*) were significantly downregulated in the transcriptome though, they were known to be downstream of *DUX4* activation<sup>8</sup>, indicating that the transcriptional decrease was caused by *DUX4*

suppression rather than the upregulation of DNA methylation and that off-target effects in the transcriptomic level were limited in spite of the potential global DNA methylation change.

As the analysis above included both “floating”, that is, not guided by dCas9/sgRNA, and “wrongly targeted” enzymatic activity, we next took another approach by starting with in silico off-target predictions to evaluate dCas9 binding based potential off-target risks (Figure 5F). The tKD-associated potential off-target probes adjacent to the 8 bp or 12 bp sequences upstream of the PAMs, obtained by the workflow detailed in Figure S5E, showed minor off-target effects in the DNA methylation level (Figure 5G, S5F, S5G). The genes with differentially upregulated probes were merged on transcriptome in relevant differentiated myocytes, showing that the global increase in DNA methylation had no major impact on gene expression (Figure 5H, S5H, Table S7). Therefore, these data suggested that even when starting the prediction with the constitutive expression of dCas9-KRAB and D3A3L, the off-target impacts on the transcriptome were limited, and the dCas9-based off-target impact was more limited. However, considering all these results, more careful attention to optimization of the balance between on-target and off-target impacts should be paid for clinical application.

## 207 **DISCUSSION**

208 In this study we have revealed that hit-and-run silencing targeting D4Z4 repeats can suppress patient-specific  
 209 endogenous *DUX4* expression beyond the distinct pathogenic genotypes of FSHD1 and FSHD2. Importantly, to the  
 210 best of our knowledge, this is the first report to edit congenital D4Z4 DNA hypomethylation to hypermethylation that  
 211 is comparable to non-FSHD levels in FSHD patient-derived cells. While even constitutive expression of single  
 212 dCas9-KRAB, dCas9-D3A, or dCas9-D3A3L could increase DNA methylation in a limited range on D4Z4 repeats,  
 213 transient activity of combined KRAB and D3A3L could have a stronger impact and spreading effect on regions distal  
 214 to sgRNA sites, suggesting synergistic effects which are not achievable with single effector applications, and this is  
 215 consistent with previous research that has aimed to target a single locus<sup>42,44</sup>. In contrast to targeting a single locus by  
 216 one time transfection, as was reported previously with hit-and-run silencing, hit-and-run activity was required several  
 217 times in our case to suppress *DUX4*; this may have been because multiple D4Z4 repeats on the whole genome were  
 218 equally targeted, limiting the capacity of enzymatic activity to influence average levels per D4Z4 unit at one time.  
 219 The D4Z4 repeats in non-FSHD are epigenetically characterized, not only by DNA hypermethylation but also by the  
 220 accumulation of the heterochromatin marker H3K9 tri-methylation/HP1 gamma,<sup>49</sup> and form distinct genome  
 221 structures outside the repeats<sup>50-54</sup>, which are reduced and abnormally rearranged respectively in FSHD. As our  
 222 epigenetic silencing strategy achieved D4Z4 repeats with hypermethylation to non-FSHD levels, it would be  
 223 interesting to further investigate whether the strategy could reconstruct non-FSHD like heterochromatin structures in  
 224 the muscle cells directly through DNA hypermethylation, which role in pathology remains controversial<sup>55</sup>.

225

At present there are several reported methods for FSHD therapy and they all have a strong focus on suppressing *DUX4* transcription or translation. Chemical compound administration for RNA interference or blocking signal transduction promisingly reduced *DUX4* expression<sup>15–19</sup>, but could result in possible disadvantages such as a need for semi-permanent frequent drug administration due to chemical instability, reduced specificity, and unknown long-term side effects due to the targeting of multifunctional signal pathways in a systemic manner. These may, however, be overcome by the hit-and-run silencing strategy with minimum repeated administration, possibly reducing hospital visits and financial burden, and consequently improving the medical and daily circumstances associated with FSHD treatment. Genome editing should be utilized further to better understand permanent transcriptional repression, but it is still technically challenging to edit the D4Z4 repeat. While editing exon3(PAS) outside of the D4Z4 repeat is technically promising for treatment, unfortunately, two groups have found unexpected *DUX4* mRNA switch phenomenon for which the mechanism is unclear<sup>20,21</sup>. Given the unexpectedly switched transcripts and the general concerns of potential on/off-targets leading to unnatural mutations, the epigenetic silencing strategy described in this investigation, appears to be more effective for *DUX4* silencing, and is safer and more containable. Moreover, our current understanding of the mechanism by which *DUX4* is activated, specifically in FSHD muscle cells, is limited. Several signaling pathways have been revealed in a context-dependent manner<sup>47,56–60</sup>. In this sense, to reconstruct the chromatin situation in patient nuclei potentially by our approach could be a more inclusive way to render the *DUX4* locus insensitive to any environmental stimulations. This might be more emphasized by imagining that patients experience excessive exhaustion or damage to their muscle when unable to access chemical compound drugs, considering that *DUX4* is strongly activated during differentiation and muscle regeneration<sup>9,61</sup>.

245

246 Our off-target analysis with EPIC array data combined with RNA-seq data showed minor impacts on the  
247 transcriptome in the non-targeted regions with the hit-and-run DNA methylation targeting. The off-target effects on  
248 the DNA methylation level were not ignorable, however, most of the differentially unregulated methylation, did not  
249 apparently depend on off-target binding candidate sites, as no apparent bias of enrichment in the off-target associated  
250 probes was observed (Figure 5G, lower panel). The constitutive expression of the dCas9-effectors in the EPIC array  
251 samples, indicated that the large off-target effects observed in this analysis were mainly derived from “floating”  
252 enzymatic effectors rather than wrongly targeted dCas9, which may be prevented by optimization of the delivery  
253 method to control the amount and active period of dCas9-effectors. Moreover, though we applied four validated  
254 sgRNAs against D4Z4 at the same time to establish the proof of concept, among them, a minimum of one sufficient  
255 for robust *DUX4* suppression should be carefully selected for future clinical applications, which may also help to  
256 minimize dCas9-guided off-target effects. Hit-and-run off-target silencing, if it happens, could also possibly cause  
257 robust and long-term impacts, which should be avoided in terms of safety in clinical situations. Moreover, intergenic  
258 regulatory regions have recently been proven to have pathogenic potentials due to disrupted fine tuning, especially  
259 in humans<sup>62,63</sup>. In this sense, in the context of future clinical use, higher coverage methods such as bisulfite high-  
260 throughput sequencing-based off-target analysis can be applied to strictly evaluate off-target risks in a sustainable  
261 manner to allow for future re-analysis for *de novo* identified naive sites.

262

263 We have shown that hit-and-run silencing worked in FSHD patient-derived cells in a proliferative pluripotent state

264 and the effect was tolerant in cell divisions for at least two weeks (maximally 10 weeks in our one trial, data not  
265 shown) and muscle differentiation, suggesting that epigenetically robust and inheritable chromatin structures were  
266 maintained beyond cell types. However, assuming the clinical application, it remains unclear whether induction of  
267 hit-and-run silencing can be achieved with the benefit of long-term effects in various kinds of myogenic cells residing  
268 in the skeletal muscle tissues, such as quiescent satellite cells, proliferative myoblasts, and terminally differentiated  
269 myofibers. Considering the spike-like activation of *DUX4* in a sporadic manner during differentiation in FSHD  
270 muscle cells and regeneration in an FSHD mouse model containing FSHD patient-derived contracted D4Z4  
271 repeats<sup>9,61</sup>, the high efficiency of transfection and sustainable effects covering satellite cells will be required to  
272 suppress disease progression in FSHD muscles. Though AAV vectors are considered to be a promising delivery  
273 method into muscle tissues due to their high efficiency<sup>35</sup>, they have a limited capacity for packaging, and moreover  
274 recent reports have raised potential risks in clinical use in terms of lethal liver dysfunction and immunogenicity<sup>34,64</sup>.  
275 Considering that one of the benefits of hit-and-run silencing is that there is no need of dCas9s/sgRNAs components  
276 to remain in the nuclei for long-term effects, it has high potential in clinical application when combined with less  
277 toxic *in vivo* transfection methods,<sup>65,66</sup> as it allows for the removal of any artificial components out of patient bodies  
278 after induction. In this sense, customized local applications targeting critical muscles for each patient's demands  
279 rather than a systemic approach will be suitable, which will fit various tendencies in the symptoms of FSHD  
280 individuals<sup>67</sup> and also help to achieve minimal side-effects in other tissues. In addition, as the hit-and-run epigenetic  
281 approach does not manipulate DNA sequences, there are fewer ethical issues than with direct genetic approaches, as  
282 it does not have the potential to produce artificial sequences through unnatural processes.



283

284 In summary, here we have proven that the hit-and-run silencing strategy for *DUX4* can work in in vitro FSHD patient  
 285 cells with minimal off-target risks. This may be a promising option by which to avoid clinical obstacles and provide  
 286 well-balanced treatment to individuals with FSHD, motivating the need for future development studies combined  
 287 with suitable delivery methods and *in vivo* models to establish further proof of concept, sufficient for clinical  
 288 application.

289

290

## 291 MATERIALS AND METHODS

### 292 Ethical approval

293 This study was approved by the Ethics Committee of the Graduate School of Medicine, Kyoto University, and the  
294 Kyoto University Hospital (Approval #R0091 and #G259) and was conducted according to the guidelines of the  
295 Declaration of Helsinki. To protect confidentiality, all patient information was kept anonymous, and written informed  
296 consent was obtained from the study participants.

### 297 Vector construction

298 The dCas9-KRAB(BFP) vector (ID: VB190207-1015wke, VectorBuilder Japan) was originally designed and created  
299 using an online design tool (<https://www.vectorbuilder.jp/design.html>) with a PiggyBac backbone and a dCas9-  
300 effector driven by a CAG promoter followed by internal ribosome entry site (IRES) and blue fluorescent protein  
301 (TagBFP). The KRAB domain was sandwiched by EcoRI and AgeI restriction enzyme sites, which enabled the  
302 insertion of all other alternative effector domains including D3A (amplified open reading frame, ORF, from Addgene  
303 #66819), D3B (amplified ORF from Addgene #66820), D3L (amplified ORF from Addgene #35523), and a negative  
304 control sequence. The dCas9-D3A3L(BFP) vector was built by adding the D3L C-terminal domain ORF after the  
305 D3A domain on dCas9-D3A(BFP). Sequence ranges for each of the DNMT3A, DNMT3B, and DNMT3L domains  
306 were based on those in a previous report<sup>68</sup>. The dCas9-KRAB(Neo) vector was created by replacing the TagBFP of  
307 dCas9-KRAB(BFP) with a neomycin resistance gene, while dCas9-Neg(Neo) was built by replacing KRAB with a  
308 negative control sequence. The backbone of the single guide RNA (sgRNA) vectors was built by removing the  
309 hygromycin resistance gene from pPV-H1-ccdb-Ef1a-RiH\_Ver1, and was provided by Dr. Akitsu Hotta (CiRA,

Kyoto University, Japan), then insertion of the sgRNA fragments was conducted as previously described<sup>69</sup>. Effector sites and sgRNA targets are summarized in Supplementary Table.S1 and Supplementary Table.S2, respectively.

# **Human iPSCs and muscle cell differentiation**

Intact human iPSC clones from one male FSHD1 patient, one female FSHD2 patient for treatments with dCas9-effectors, one male FSHD2 patient for the control, specified as No Vector in the global methylation study, and one non-FSHD donor were used in this research and were originally described in a previous study<sup>47</sup>. Non-FSHD healthy S01 was generated under written consent with approval of the Kyoto University Graduate School and Faculty of Medicine Ethics Committee (approval nos. E1762, G567, and Rinsho71). iPSC clones with the doxycycline-inducible MyoD transgene (iPS<sup>tet-MyoD</sup> clones) were established by transfecting them with plasmids, including PBase and PB-MyoD (with puromycin resistance marker) and sub-cloning one of those that showed the highest level of differentiation efficiency. All human iPSC clones were cultured and maintained under feeder-free culture conditions as previously described<sup>70</sup>. Briefly, the cells were passaged once a week and cultured on an iMatrix-511 (Nippi, Japan) pre-coated dish in StemFit AK02N medium (Ajinomoto). Then, 0.5 µg/mL puromycin (Nacalai Tesque, Japan) or 100 µg/mL neomycin sulfate (Nacalai Tesque) was added for selection and maintenance of the relevant transgenes. Muscle cell differentiation was performed as described previously<sup>71</sup> with some modifications. Briefly, at day 0, iPS<sup>tet-MyoD</sup> cells were treated with accutase (Nacalai Tesque) to separate them into single cells and were plated at a density of  $2\text{--}2.5 \times 10^5$  cells/well in 6-well dishes coated with Matrigel (Corning, NY) in StemFit supplemented with 10 µM Y-27632 (Nacalai Tesque). At day 1, medium was replaced with primate ES cell medium (REPROCELL, Japan). at day 2, the culture medium was replaced with primate ES cell medium containing 1 µg/mL doxycycline (Dox; LKT

Laboratories, MN). Induction was performed in 5% KSR/ $\alpha$ -MEM containing a Dox and 2-mercaptoethanol (2-ME) supplement without replating at day 3 for 3 days (FSHD1 clones) or 4 days (FSHD2 clones). After induction, cells were matured in 5% KSR/ $\alpha$ -MEM containing 2-ME, 10 ng/mL human IGF-1 (Pepro Tech, UK), and 5 $\mu$ M SB431542 (Wako, Japan) until day 9 (FSHD1 clones) or day 10 (FSHD2 clones).

### **Electroporation**

Electroporation was performed using a NEPA21 electroporator (Nepa Gene, Japan) into human iPS cells. According to the following conditions: 2  $\mu$ g of an sgRNAs mixture that consists of 500 ng of each of the four sgRNA vectors, 12–13  $\mu$ g of dCas9 vectors and 1  $\mu$ g of PBase were co-transfected into  $1 \times 10^6$  cells per 100  $\mu$ L Opti-MEM (Thermo Fisher Scientific, Japan) per cuvette, as was described previously<sup>47</sup>.

### **Fluorescence activating cell sorter (FACS) analysis and sorting**

Cells were dissociated by accutase, washed once in StemFit medium containing 10  $\mu$ M Y-27632, and resuspended in Hanks' Balanced Salt Solution (HBSS) containing 10  $\mu$ M Y-27632 and approximately 5% of the StemFit medium which was roughly carried over from the washing, filtered, and kept on ice. Cells were analyzed and sorted for RFP and BFP with Aria II (BD Biosciences). Cells were then collected in culture medium with Y-27632 at 4°C and replated for expansion. After expansion, cells were observed to capture images of phased contrast and fluorescence using a BZ9000 system (Keyence, Japan) at 200 $\times$  magnification.

### **RNA extraction and real-time reverse-transcription quantitative PCR (RT-qPCR)**

Total RNA was extracted using a ReliaPrep RNA Miniprep System (Promega, WI) as per the manufacturer's instructions. cDNA was synthesized from the extracted RNA using a ReverTra Ace Master Mix with gDNA Remover

(TOYOBO, Japan). Real-time RT-qPCR was performed using SYBR Green probe sets (Applied Biosystems, MA) and a Step One Plus thermal cycler (Applied Biosystems), and a standard curve was prepared for each target. *RPLP0*, which encodes a ribosomal protein, was used as the internal control in all assays. The primer sets used in this study are listed in Supplementary Table.S3. All the RT-qPCR data were processed with GraphPad Prism 8 for visualization and statistical analysis and were represented as mean  $\pm$  SEM. P values were determined using one way ANOVA followed by the Tukey's multiple comparisons test with  $P \leq 0.05$  considered as statistically significant.

### **RNA-seq**

Total RNA was obtained from sorted cells using the ReliaPrep RNA Cell Miniprep System (Promega). RNA quality was evaluated using a NanoDrop 2000 (Thermo Fisher Scientific) and Agilent 2100 Bioanalyzer System (Agilent) with an RNA Pico Kit (Agilent, CA) according to the manufacture's instruction. For the Illumina sequencing libraries, 5 ng of total RNA was used with the SMARTer Stranded Total RNA-Seq Kit v3 - Pico Input Mammalian (TAKARA, Japan), according to the manufacture's instruction. The libraries were quantified using the Agilent 2100 Bioanalyzer System with a High Sensitivity DNA Kit (Agilent) according to the manufacture's instruction, and equal amounts from molecular pools were used for RNA-seq analysis, using a Next seq 500 (Illumina, CA) in the paired-end mode with 144 bp : 8 bp : 8 bp : 8 bp for R1:l1:l2:R2. The raw sequence data were converted to fastq files, and the sequenced reads of R1 were trimmed to remove adaptors and low-quality bases using Cutadapt with '-m 20 --nextseq-trim=20' option. The 8bp sequences of R2 were transferred as unique molecular identifiers (UMIs) to each corresponding strand name in R1 reads using UMI-tools extract function. Then R1 reads were mapped to the reference human genome GRCh38, which downloaded from the NCBI RefSeq, using STAR<sup>72</sup>. Deduplication was conducted using

UMI-tools dedup function. After deduplication, HTSeq<sup>73</sup> was used to calculate gene read counts, and the counted data were normalized by DEseq2<sup>74</sup>. Lists of annotated genes associated to DUX4 downstream activation and myogenic differentiation were cited from previous work<sup>75</sup> and a Gene Set Enrichment Analysis (GSEA) library<sup>76</sup> (HALLMARK\_MYOGENESIS, M5909), respectively. For visualization, EnhancedVolcano (Blighe, Rana, and Lewis, 2018) was utilized to generate volcano plots. Gene names are shown in Supplementary Table.S4.

### **Targeted DNA methylation analysis using bisulfite sanger sequencing**

Genomic DNA was extracted using a GenElute Mammalian Genomic DNA Miniprep Kit (Sigma-Aldrich, MO) as per the manufacturer's protocol, and 500 ng to 1 µg of DNA was treated with bisulfite using an EpiTect DNA bisulfite kit (QIAGEN, Germany) according to the manufacturer's guidelines. PCR and DNA methylation analysis of the *DUX4* 5' promoter region was performed according to the protocol of the *DUX4* 5' BSS assay, as described previously<sup>48</sup> with QUMA online software ([http://quma.cdb.riken.jp/index\\_j.html](http://quma.cdb.riken.jp/index_j.html))<sup>77</sup>; the analysis was performed with the parameters as follows; upper limit of unconverted CpGs = 5, lower limit of percent converted CpGs = 95.0, upper limit of alignment mismatches = 30, lower limit of percent identity = 90.0. The averaged DNA methylation percentages for each CpG site were summarized as heatmaps with GraphPad Prism 8.

### **Global DNA methylation analysis with EPIC array data**

The Infinium MethylationEPIC BeadChip Kit (illumina) was utilized in accordance with the manufacturer's protocol in the faculty department of the CiRA Foundation, Kyoto University, Japan. First, 500 ng of genomic DNA was bisulfite converted using an EZ DNA Methylation Kit (ZYMO RESEARCH, CA) and the DNA methylation level was quantified using EPIC BeadChIP (Illumina) run on an Illumina iScan System according to the manufacturer's

guidelines. Raw IDAT files were processed using the ChAMP package (v. 2.21.1) in R for filtering, normalization was conducted using champ.norm (arraytype = "EPIC") and calculations with the function champ.DMP (arraytype = "EPIC") to generate methylation  $\beta$ -values and calculate adjusted p-values for significant DMPs<sup>78</sup>. Among all the probes covering over 850,000 sites, 718 165 probes remained with DNA methylation levels obtained after filtering and normalizing. Significant DMPs were selected using the following criteria:  $> 0.2$   $\beta$ -value gap and  $< 0.05$  adjusted p-value. PCA analysis was performed using DNA methylation data from all probes in R.

### ***in silico* off-target prediction**

The 23 bp (20bp + 3bp PAM) sequences of each sgRNA were submitted to the online CRISPRdirect tool<sup>79</sup> to obtain the off-target candidate sites that match the 20 mer / 12 mer / 8 mer + NGG(PAM) on GRCh37 as a BED file and loaded in R. All the sites that matched the 8 bp or 12 bp sequences upstream of the PAM were selected as potential binding sites. Infinium MethylationEPIC v1.0 B5 Manifest File (CSV Format) was loaded in R and only probes that remained after filtering were formatted into genomic ranges with gene annotations. The approximate probes within 500 bp of each site were selected by applying the findOverlaps() function among off-target candidate sites and manifest file accompanied with gene annotation and filtered using the criteria of a  $< 500$  bp distance. This *in silico* workflow was confirmed with a newly designed sgRNA target against MyoG promotor as a virtual example to successfully pick up MyoG gene and other potential off-target genes (Figure S5E). The code for the prediction process is available in GitHub ([https://github.com/mits2112/offtarget\\_predict\\_EPICarray](https://github.com/mits2112/offtarget_predict_EPICarray)). The selected probes were emphasized in the dot plots. Gene annotations were used as off-target candidate genes if the relevant probe satisfied the criteria for significant difference with a  $> 0.2$  beta value gap and  $< 0.05$  adjusted p-value.

## AUTHOR CONTRIBUTION

The whole concept and experimental design were made by M.SH. and H.S. Culture works including FACS were performed by M.SH. and J.H.. DNA/RNA works were performed by M.SH. and M.A.. Library preparation and NGS run were performed by M.SH., T.J., K.O. and T.Y.. Analysis of NGS data was processed by M.SH., S.S. and T.Y.. Analysis of EPIC array data was processed by M.SH. The manuscript was prepared by M.SH., J.H. and H.S.

## ACKNOWLEDGEMENTS

We are grateful to the donors who gave their cells for the establishment of iPSCs used in this study. We thank Mr. Masaki Nomura, Mrs. Hiromi Dohi and Mrs. Maki Hira at the faculty of CiRA Foundation for performing DNA methylationEPIC array protocol. We thank Dr. Akitsu Hotta (CiRA), Dr. Stanly Qi (Stanford University, Stanford, California), Dr. Peter L. Jones (University of Nevada, NV) and Mr. Jun Otomo for critical comments to our study, Dr. Kanae Mitsunaga for technical support of FACS and Dr. Chikako Okubo (CiRA) for technical support of NGS data analysis. We would like to thank Editage ([www.editage.com](http://www.editage.com)) for English language editing. M.SH. appreciates all the members of his laboratory for kind supports because of his physical handicap. M.SH. especially appreciates his family and Japan FSHD patient community for generous and unwavering supports.

## SUPPLEMENTAL INFORMATION

Supplementary figures S1-S5 and supplementary tables S1-S7 are available.



424 **FUNDING**

425 This work was supported by a grant from the Acceleration Program for Intractable Diseases Research utilizing  
 426 Disease-specific iPS cells, which were provided by the Japan Agency for Medical Research and Development,  
 427 AMED (#21bm0804005h0005 to H.S.); the Japan Society for the Promotion of Science KAKENHI [20J01478 to  
 428 M.SH., and 21J11349 to J.H.]; and 2019 Grant by Fujiwara Memorial Foundation to M.SH.

429

430 **CONFLICT OF INTEREST STATEMENT**

431 The authors declare that they have no conflict of interest.

432

## REFERENCES

1. van Deutekom, J.C., Wijmenga, C., van Tienhoven, E.A., Gruter, A.M., Hewitt, J.E., Padberg, G.W., van Ommen, G.J., Hofker, M.H., and Frants, R.R. (1993). FSHD associated DNA rearrangements are due to deletions of integral copies of a 3.2 kb tandemly repeated unit. *Hum. Mol. Genet.* 2, 2037–2042.
2. Lemmers, R.J.L.F., Tawil, R., Petek, L.M., Balog, J., Block, G.J., Santen, G.W.E., Amell, A.M., Van Der Vliet, P.J., Almomani, R., Straasheijm, K.R., et al. (2012). Digenic inheritance of an SMCHD1 mutation and an FSHD-permissive D4Z4 allele causes facioscapulohumeral muscular dystrophy type 2. *Nat. Genet.* 44, 1370–1374.
3. Van Den Boogaard, M.L., Lemmers, R.J.L.F., Balog, J., Wohlgemuth, M., Auranen, M., Mitsuhashi, S., Van Der Vliet, P.J., Straasheijm, K.R., Van Den Akker, R.F.P., Kriek, M., et al. (2016). Mutations in DNMT3B Modify Epigenetic Repression of the D4Z4 Repeat and the Penetrance of Facioscapulohumeral Dystrophy. *Am. J. Hum. Genet.* 98, 1020–1029.
4. Hamanaka, K., Šikrová, D., Mitsuhashi, S., Masuda, H., Sekiguchi, Y., Sugiyama, A., Shibuya, K., Lemmers, R.J.L.F., Goossens, R., Ogawa, M., et al. (2020). Homozygous nonsense variant in *LRIF1* associated with facioscapulohumeral muscular dystrophy. *Neurology* 94, e2441–e2447.
5. Gabriëls, J., Beckers, M.C., Ding, H., De Vriese, A., Plaisance, S., van der Maarel, S.M., Padberg, G.W., Frants, R.R., Hewitt, J.E., Collen, D., et al. (1999). Nucleotide sequence of the partially deleted D4Z4 locus in a patient with FSHD identifies a putative gene within each 3.3 kb element. *Gene* 236, 25–32.
6. Lemmers, R.J.L.F., van der Vliet, P.J., Klooster, R., Sacconi, S., Camaño, P., Dauwerse, J.G., Snider, L.,

- 452 Straasheijm, K.R., van Ommen, G.J., Padberg, G.W., et al. (2010). A unifying genetic model for
- 453 facioscapulohumeral muscular dystrophy. *Science* 329, 1650–1653.
- 454 7. Snider, L., Geng, L.N., Lemmers, R.J.L.F., Kyba, M., Ware, C.B., Nelson, A.M., Tawil, R., Filippova, G.N., van
- 455 der Maarel, S.M., Tapscott, S.J., et al. (2010). Facioscapulohumeral Dystrophy: Incomplete Suppression of a
- 456 Retrotransposed Gene. *PLOS Genet.* 6, e1001181.
- 457 8. Geng, L.N., Yao, Z., Snider, L., Fong, A.P., Cech, J.N., Young, J.M., VanderMaarel, S.M., Ruzzo, W.L.,
- 458 Gentleman, R.C., Tawil, R., et al. (2012). DUX4 Activates Germline Genes, Retroelements, and Immune
- 459 Mediators: Implications for Facioscapulohumeral Dystrophy. *Dev. Cell* 22, 38–51.
- 460 9. Rickard, A.M., Petek, L.M., and Miller, D.G. (2015). Endogenous DUX4 expression in FSHD myotubes is
- 461 sufficient to cause cell death and disrupts RNA splicing and cell migration pathways. *Hum. Mol. Genet.* 24,
- 462 5901–5914.
- 463 10. Bosnakovski, D., Gearhart, M.D., Toso, E.A., Ener, E.T., Choi, S.H., and Kyba, M. (2018). Low level DUX4
- 464 expression disrupts myogenesis through deregulation of myogenic gene expression. *Sci. Rep.* 8, 16957.
- 465 11. Cohen, J., DeSimone, A., Lek, M., and Lek, A. (2021). Therapeutic Approaches in Facioscapulohumeral
- 466 Muscular Dystrophy. *Trends Mol. Med.* 27, 123–137.
- 467 12. Lim, K.R.Q., and Yokota, T. (2021). Genetic Approaches for the Treatment of Facioscapulohumeral Muscular
- 468 Dystrophy . *Front. Pharmacol.* 12.
- 469 13. Bou Saada, Y., Dib, C., Dmitriev, P., Hamade, A., Carnac, G., Laoudj-Chenivresse, D., Lipinski, M., and
- 470 Vassetzky, Y.S. (2016). Facioscapulohumeral dystrophy myoblasts efficiently repair moderate levels of oxidative

- 471 DNA damage. *Histochem. Cell Biol.* *145*, 475–483.
- 472 14. Banerji, C.R.S., and Zammit, P.S. (2021). Pathomechanisms and biomarkers in facioscapulohumeral muscular  
473 dystrophy: roles of DUX4 and PAX7. *EMBO Mol. Med.* *13*, e13695.
- 474 15. Anseau, E., Vanderplanck, C., Wauters, A., Harper, S.Q., Coppée, F., and Belayew, A. (2017). Antisense  
475 Oligonucleotides Used to Target the DUX4 mRNA as Therapeutic Approaches in FaciosScapuloHumeral  
476 Muscular Dystrophy (FSHD). *Genes (Basel)*. *8*.
- 477 16. Bouwman, L.F., den Hamer, B., van den Heuvel, A., Franken, M., Jackson, M., Dwyer, C.A., Tapscott, S.J.,  
478 Rigo, F., van der Maarel, S.M., and de Greef, J.C. (2021). Systemic delivery of a DUX4-targeting antisense  
479 oligonucleotide to treat facioscapulohumeral muscular dystrophy. *Mol. Ther. Nucleic Acids* *26*, 813–827.
- 480 17. Lim, K.R.Q., Maruyama, R., Echigoya, Y., Nguyen, Q., Zhang, A., Khawaja, H., Sen Chandra, S., Jones, T.,  
481 Jones, P., Chen, Y.-W., et al. (2020). Inhibition of DUX4 expression with antisense LNA gapmers as a therapy  
482 for facioscapulohumeral muscular dystrophy. *Proc. Natl. Acad. Sci. U. S. A.* *117*, 16509–16515.
- 483 18. Lim, K.R.Q., Bittel, A., Maruyama, R., Echigoya, Y., Nguyen, Q., Huang, Y., Dzierlega, K., Zhang, A., Chen,  
484 Y.-W., and Yokota, T. (2021). DUX4 Transcript Knockdown with Antisense 2'-O-Methoxyethyl Gapmers for  
485 the Treatment of Facioscapulohumeral Muscular Dystrophy. *Mol. Ther.* *29*, 848–858.
- 486 19. Oliva, J., Galasinski, S., Richey, A., Campbell, A.E., Meyers, M.J., Modi, N., Zhong, J.W., Tawil, R., Tapscott,  
487 S.J., and Sverdrup, F.M. (2019). Clinically Advanced p38 Inhibitors Suppress DUX4 Expression in Cellular and  
488 Animal Models of Facioscapulohumeral Muscular Dystrophy. *J. Pharmacol. Exp. Ther.* *370*, 219–230.
- 489 20. Joubert, R., Mariot, V., Charpentier, M., Concordet, J.P., and Dumonceaux, J. (2021). Gene Editing Targeting the

490 DUX4 Polyadenylation Signal: A Therapy for FSHD? *J. Pers. Med.* 11.

491 21. Šikrová, D., Cadar, V.A., Ariyurek, Y., Laros, J.F.J., Balog, J., and van der Maarel, S.M. (2021). Adenine base  
492 editing of the DUX4 polyadenylation signal for targeted genetic therapy in facioscapulohumeral muscular  
493 dystrophy. *Mol. Ther. - Nucleic Acids* 25, 342–354.

494 22. Akatsuka, K., Sasaki-Honda, M., and Sawai, T. (2020). Ethical Framework for Next-Generation Genome and  
495 Epigenome Editing. *Am. J. Bioeth.* 20, 32–36.

496 23. Cwik, B. (2020). Revising, Correcting, and Transferring Genes. *Am. J. Bioeth.* 20, 7–18.

497 24. Greco, A., Goossens, R., van Engelen, B., and van der Maarel, S.M. (2020). Consequences of epigenetic  
498 derepression in facioscapulohumeral muscular dystrophy. *Clin. Genet.* 97, 799–814.

499 25. Qi, L.S., Larson, M.H., Gilbert, L.A., Doudna, J.A., Weissman, J.S., Arkin, A.P., and Lim, W.A. (2013).  
500 Repurposing CRISPR as an RNA-guided platform for sequence-specific control of gene expression. *Cell* 152,  
501 1173–1183.

502 26. Gilbert, L.A., Larson, M.H., Morsut, L., Liu, Z., Brar, G.A., Torres, S.E., Stern-Ginossar, N., Brandman, O.,  
503 Whitehead, E.H., Doudna, J.A., et al. (2013). CRISPR-mediated modular RNA-guided regulation of transcription  
504 in eukaryotes. *Cell* 154, 442–451.

505 27. Adli, M. (2018). The CRISPR tool kit for genome editing and beyond. *Nat. Commun.* 9.

506 28. Liu, X.S., Wu, H., Ji, X., Stelzer, Y., Wu, X., Czauderna, S., Shu, J., Dadon, D., Young, R.A., and Jaenisch, R.  
507 (2016). Editing DNA Methylation in the Mammalian Genome. *Cell* 167, 233–247.e17.

508 29. Liu, X.S., Wu, H., Krzisch, M., Wu, X., Graef, J., Muffat, J., Hnisz, D., Li, C.H., Yuan, B., Xu, C., et al. (2018).

509 Rescue of Fragile X Syndrome Neurons by DNA Methylation Editing of the FMR1 Gene. *Cell* 172, 979-992.e6.

510 30. Kemaladewi, D.U., Bassi, P.S., Erwood, S., Al-Basha, D., Gawlik, K.I., Lindsay, K., Hyatt, E., Kember, R.,  
511 Place, K.M., Marks, R.M., et al. (2019). A mutation-independent approach for muscular dystrophy via  
512 upregulation of a modifier gene. *Nature* 572, 125–130.

513 31. Himeda, C.L., Jones, T.I., and Jones, P.L. (2016). CRISPR/dCas9-mediated transcriptional inhibition ameliorates  
514 the epigenetic dysregulation at D4Z4 and represses DUX4-fl in FSH muscular dystrophy. *Mol. Ther.* 24, 527–  
515 535.

516 32. Himeda, C.L., Jones, T.I., and Jones, P.L. (2021). Targeted epigenetic repression by CRISPR/dSaCas9  
517 suppresses pathogenic DUX4-fl expression in FSHD. *Mol. Ther. - Methods Clin. Dev.* 20, 298–311.

518 33. Bintu, L., Yong, J., Antebi, Y.E., McCue, K., Kazuki, Y., Uno, N., Oshimura, M., and Elowitz, M.B. (2016).  
519 Dynamics of epigenetic regulation at the single-cell level. *Science* (80-. ). 351, 720–724.

520 34. Hakim, C.H., Kumar, S.R.P., Pérez-López, D.O., Wasala, N.B., Zhang, D., Yue, Y., Teixeira, J., Pan, X., Zhang,  
521 K., Million, E.D., et al. (2021). Cas9-specific immune responses compromise local and systemic AAV CRISPR  
522 therapy in multiple dystrophic canine models. *Nat. Commun.* 12, 6769.

523 35. Crudele, J.M., and Chamberlain, J.S. (2019). AAV-based gene therapies for the muscular dystrophies. *Hum. Mol.*  
524 *Genet.* 28, R102–R107.

525 36. Manini, A., Abati, E., Nuredini, A., Corti, S., and Comi, G. Pietro (2022). Adeno-Associated Virus (AAV)-  
526 Mediated Gene Therapy for Duchenne Muscular Dystrophy: The Issue of Transgene Persistence . *Front.*  
527 *Neurol.* 12.

528 37. High-dose AAV gene therapy deaths (2020). *Nat. Biotechnol.* 38, 910.

529 38. Philippidis, A. (2022). After Patient Death, FDA Places Hold on Pfizer Duchenne Muscular Dystrophy Gene  
530 Therapy Trial. *Hum. Gene Ther.* 33, 111–115.

531 39. O’Geen, H., Ren, C., Nicolet, C.M., Perez, A.A., Halmai, J., Le, V.M., MacKay, J.P., Farnham, P.J., and Segal,  
532 D.J. (2017). dCas9-based epigenome editing suggests acquisition of histone methylation is not sufficient for  
533 target gene repression. *Nucleic Acids Res.* 45, 9901–9916.

534 40. Vojta, A., Dobrinic, P., Tadic, V., Bockor, L., Korac, P., Julg, B., Klasic, M., and Zoldos, V. (2016).  
535 Repurposing the CRISPR-Cas9 system for targeted DNA methylation. *Nucleic Acids Res.* 44, 5615–5628.

536 41. Saunderson, E.A., Stepper, P., Gomm, J.J., Hoa, L., Morgan, A., Allen, M.D., Jones, J.L., Gribben, J.G.,  
537 Jurkowski, T.P., and Ficuz, G. (2017). Hit-and-run epigenetic editing prevents senescence entry in primary breast  
538 cells from healthy donors. *Nat. Commun.* 8, 1–14.

539 42. Amabile, A., Migliara, A., Capasso, P., Biffi, M., Cittaro, D., Naldini, L., and Lombardo, A. (2016). Inheritable  
540 Silencing of Endogenous Genes by Hit-and-Run Targeted Epigenetic Editing. *Cell* 167, 219-232.e14.

541 43. Stepper, P., Kungulovski, G., Jurkowska, R.Z., Chandra, T., Krueger, F., Reinhardt, R., Reik, W., Jeltsch, A., and  
542 Jurkowski, T.P. (2017). Efficient targeted DNA methylation with chimeric dCas9-Dnmt3a-Dnmt3L  
543 methyltransferase. *Nucleic Acids Res.* 45, 1703–1713.

544 44. O’Geen, H., Bates, S.L., Carter, S.S., Nisson, K.A., Halmai, J., Fink, K.D., Rhie, S.K., Farnham, P.J., and Segal,  
545 D.J. (2019). Ezh2-dCas9 and KRAB-dCas9 enable engineering of epigenetic memory in a context-dependent  
546 manner. *Epigenetics and Chromatin* 12, 1–20.

547 45. Nuñez, J.K., Chen, J., Pommier, G.C., Cogan, J.Z., Replogle, J.M., Adriaens, C., Ramadoss, G.N., Shi, Q., Hung,  
548 K.L., Samelson, A.J., et al. (2021). Genome-wide programmable transcriptional memory by CRISPR-based  
549 epigenome editing. *Cell* 184, 2503-2519.e17.

550 46. Mlambo, T., Nitsch, S., Hildenbeutel, M., Romito, M., Müller, M., Bossen, C., Diederichs, S., Cornu, T.I.,  
551 Cathomen, T., and Mussolino, C. (2018). Designer epigenome modifiers enable robust and sustained gene  
552 silencing in clinically relevant human cells. *Nucleic Acids Res.* 46, 4456–4468.

553 47. Sasaki-Honda, M., Jonouchi, T., Arai, M., Hotta, A., Mitsunashi, S., Nishino, I., Matsuda, R., and Sakurai, H.  
554 (2018). A patient-derived iPSC model revealed oxidative stress increases facioscapulohumeral muscular  
555 dystrophy-causative DUX4. *Hum. Mol. Genet.* 27, 4024–4035.

556 48. Jones, T.I., Yan, C., Sapp, P.C., McKenna-Yasek, D., Kang, P.B., Quinn, C., Salameh, J.S., King, O.D., and  
557 Jones, P.L. (2014). Identifying diagnostic DNA methylation profiles for facioscapulohumeral muscular dystrophy  
558 in blood and saliva using bisulfite sequencing. *Clin. Epigenetics* 6, 23.

559 49. Zeng, W., De Greef, J.C., Chen, Y.Y., Chien, R., Kong, X., Gregson, H.C., Winokur, S.T., Pyle, A., Robertson,  
560 K.D., Schmiesing, J.A., et al. (2009). Specific loss of histone H3 lysine 9 trimethylation and HP1 $\gamma$ /cohesin  
561 binding at D4Z4 repeats is associated with facioscapulohumeral dystrophy (FSHD). *PLoS Genet.* 5.

562 50. Bodega, B., Ramirez, G.D.C., Grasser, F., Cheli, S., Brunelli, S., Mora, M., Meneveri, R., Marozzi, A., Mueller,  
563 S., Battaglioli, E., et al. (2009). Remodeling of the chromatin structure of the facioscapulohumeral muscular  
564 dystrophy (FSHD) locus and upregulation of FSHD-related gene 1 (FRG1) expression during human myogenic  
565 differentiation. *BMC Biol.* 7, 41.



566 51. Pirozhkova, I., Petrov, A., Dmitriev, P., Laoudj, D., Lipinski, M., and Vassetzky, Y. (2008). A functional role for  
567 4qA/B in the structural rearrangement of the 4q35 region and in the regulation of FRG1 and ANT1 in  
568 facioscapulohumeral dystrophy. *PLoS One* 3, e3389.

569 52. Cortesi, A., Pesant, M., Sinha, S., Marasca, F., Sala, E., Gregoretti, F., Antonelli, L., Oliva, G., Chiereghin, C.,  
570 Soldà, G., et al. (2019). 4q-D4Z4 chromatin architecture regulates the transcription of muscle atrophic genes in  
571 facioscapulohumeral muscular dystrophy. *Genome Res.* 29, 883–895.

572 53. Robin, J.D., Ludlow, A.T., Batten, K., Gaillard, M.-C., Stadler, G., Magdinier, F., Wright, W.E., and Shay, J.W.  
573 (2015). SORBS2 transcription is activated by telomere position effect-over long distance upon telomere  
574 shortening in muscle cells from patients with facioscapulohumeral dystrophy. *Genome Res.* 25, 1781–1790.

575 54. Gaillard, M.-C., Broucqsault, N., Morere, J., Laberthonnière, C., Dion, C., Badja, C., Roche, S., Nguyen, K.,  
576 Magdinier, F., and Robin, J.D. (2019). Analysis of the 4q35 chromatin organization reveals distinct long-range  
577 interactions in patients affected with Facio-Scapulo-Humeral Dystrophy. *Sci. Rep.* 9, 10327.

578 55. Salsi, V., Magdinier, F., and Tupler, R. (2020). Does DNA methylation matter in FSHD? *Genes (Basel)*. 11, 8–  
579 10.

580 56. Block, G.J., Narayanan, D., Amell, A.M., Petek, L.M., Davidson, K.C., Bird, T.D., Tawil, R., Moon, R.T., and  
581 Miller, D.G. (2013). Wnt/??-catenin signaling suppresses DUX4 expression and prevents apoptosis of FSHD  
582 muscle cells. *Hum. Mol. Genet.* 22, 4661–4672.

583 57. Campbell, A.E., Oliva, J., Yates, M.P., Zhong, J.W., Shadle, S.C., Snider, L., Singh, N., Tai, S., Hiramuki, Y.,  
584 Tawil, R., et al. (2017). BET bromodomain inhibitors and agonists of the beta-2 adrenergic receptor identified in

585 screens for compounds that inhibit DUX4 expression in FSHD muscle cells. *Skelet. Muscle* 7, 16.

586 58. Rojas, L.A., Valentine, E., Accorsi, A., Maglio, J., Shen, N., Robertson, A., Kazmirski, S., Rahl, P., Tawil, R.,  
587 Cadavid, D., et al. (2020). p38 $\alpha$ ; Regulates Expression of DUX4 in a Model of  
588 Facioscapulohumeral Muscular Dystrophy. *J. Pharmacol. Exp. Ther.* 374, 489 LP – 498.

589 59. Grow, E.J., Weaver, B.D., Smith, C.M., Guo, J., Stein, P., Shadle, S.C., Hendrickson, P.G., Johnson, N.E.,  
590 Butterfield, R.J., Menafrá, R., et al. (2021). p53 convergently activates Dux/DUX4 in embryonic stem cells and  
591 in facioscapulohumeral muscular dystrophy cell models. *Nat. Genet.* 53, 1207–1220.

592 60. Karpukhina, A., Tiukacheva, E., Dib, C., and Vassetzky, Y.S. (2021). Control of DUX4 Expression in  
593 Facioscapulohumeral Muscular Dystrophy and Cancer. *Trends Mol. Med.* 27, 588–601.

594 61. Knopp, P., Krom, Y.D., Banerji, C.R.S., Panamarova, M., Moyle, L.A., den Hamer, B., van der Maarel, S.M.,  
595 and Zammit, P.S. (2016). DUX4 induces a transcriptome more characteristic of a less-differentiated cell state and  
596 inhibits myogenesis. *J. Cell Sci.* 129, 3816–3831.

597 62. Kvon, E.Z., Waymack, R., Gad, M., and Wunderlich, Z. (2021). Enhancer redundancy in development and  
598 disease. *Nat. Rev. Genet.* 22, 324–336.

599 63. Sánchez-Gaya, V., Mariner-Faullí, M., and Rada-Iglesias, A. (2020). Rare or Overlooked? Structural Disruption  
600 of Regulatory Domains in Human Neurocristopathies . *Front. Genet.* 11.

601 64. Morales, L., Gambhir, Y., Bennett, J., and Stedman, H.H. (2020). Broader Implications of Progressive Liver  
602 Dysfunction and Lethal Sepsis in Two Boys following Systemic High-Dose AAV. *Mol. Ther.* 28, 1753–1755.

603 65. Kenjo, E., Hozumi, H., Makita, Y., Iwabuchi, K.A., Fujimoto, N., Matsumoto, S., Kimura, M., Amano, Y., Ifuku,

604 M., Naoe, Y., et al. (2021). Low immunogenicity of LNP allows repeated administrations of CRISPR-Cas9  
605 mRNA into skeletal muscle in mice. *Nat. Commun.* *12*, 7101.

606 66. Lee, K., Conboy, M., Park, H.M., Jiang, F., Kim, H.J., Dewitt, M.A., Mackley, V.A., Chang, K., Rao, A.,  
607 Skinner, C., et al. (2017). Nanoparticle delivery of Cas9 ribonucleoprotein and donor DNA in vivo induces  
608 homology-directed DNA repair. *Nat. Biomed. Eng.* *1*, 889–901.

609 67. Hamel, J., Johnson, N., Tawil, R., Martens, W.B., Dilek, N., McDermott, M.P., and Heatwole, C. (2019). Patient-  
610 Reported Symptoms in Facioscapulohumeral Muscular Dystrophy (PRISM-FSHD). *Neurology* *93*, e1180–e1192.

611 68. Ren, W., Gao, L., and Song, J. (2018). Structural basis of DNMT1 and DNMT3A-mediated DNA methylation.  
612 *Genes (Basel)*. *9*.

613 69. Li, H.L., Gee, P., Ishida, K., and Hotta, A. (2016). Efficient genomic correction methods in human iPS cells  
614 using CRISPR-Cas9 system. *Methods* *101*, 27–35.

615 70. Nakagawa, M., Taniguchi, Y., Senda, S., Takizawa, N., Ichisaka, T., Asano, K., Morizane, A., Doi, D.,  
616 Takahashi, J., Nishizawa, M., et al. (2014). A novel efficient feeder-free culture system for the derivation of  
617 human induced pluripotent stem cells. *Sci. Rep.* *4*, 3594.

618 71. Uchimura, T., Otomo, J., Sato, M., and Sakurai, H. (2017). A human iPS cell myogenic differentiation system  
619 permitting high-throughput drug screening. *Stem Cell Res.* *25*, 98–106.

620 72. Dobin, A., Davis, C.A., Schlesinger, F., Drenkow, J., Zaleski, C., Jha, S., Batut, P., Chaisson, M., and Gingeras,  
621 T.R. (2013). STAR: ultrafast universal RNA-seq aligner. *Bioinformatics* *29*, 15–21.

622 73. Anders, S., Pyl, P.T., and Huber, W. (2015). HTSeq—a Python framework to work with high-throughput

623 sequencing data. *Bioinformatics* 31, 166–169.

624 74. Love, M.I., Huber, W., and Anders, S. (2014). Moderated estimation of fold change and dispersion for RNA-seq  
625 data with DESeq2. *Genome Biol.* 15, 550.

626 75. Mitsuhashi, S., Nakagawa, S., Sasaki-Honda, M., Sakurai, H., Frith, M.C., and Mitsuhashi, H. (2021). Nanopore  
627 direct RNA sequencing detects DUX4-activated repeats and isoforms in human muscle cells. *Hum. Mol. Genet.*  
628 30, 552–563.

629 76. Liberzon, A., Birger, C., Thorvaldsdóttir, H., Ghandi, M., Mesirov, J.P., and Tamayo, P. (2015). The Molecular  
630 Signatures Database (MSigDB) hallmark gene set collection. *Cell Syst.* 1, 417–425.

631 77. Kumaki, Y., Oda, M., and Okano, M. (2008). QUMA: quantification tool for methylation analysis. *Nucleic Acids*  
632 *Res.* 36, 170–175.

633 78. Morris, T.J., Butcher, L.M., Feber, A., Teschendorff, A.E., Chakravarthy, A.R., Wojdacz, T.K., and Beck, S.  
634 (2014). ChAMP: 450k Chip Analysis Methylation Pipeline. *Bioinformatics* 30, 428–430.

635 79. Naito, Y., Hino, K., Bono, H., and Ui-Tei, K. (2015). CRISPRdirect: software for designing CRISPR/Cas guide  
636 RNA with reduced off-target sites. *Bioinformatics* 31, 1120–1123.

## FIGURE LEGENDS

Figure 1. Establishment and validation of dCas9-effectors for the evaluation of DUX4 suppression using the FSHD2-iPSC model. See also Figure S1.

A) Construct designs for the PiggyBac vectors used in this experiment. dCas9-effectors are driven by a CAG promoter and followed by internal ribosome entry site (IRES) connected to a blue fluorescence protein (TagBFP) element, while sgRNA vectors contained an red fluorescence protein (RFP) element. B) Scheme showing the transfection, selection, and differentiation of iPSC clones to myocytes. After FSHD2 iPSC<sup>tet-MyoD</sup> clones were transfected by electroporation, cells with constitutive BFP and RFP dual signals were sorted and differentiated for analysis. C–E) RT-qPCR analysis for C) DUX4-fl, D) DUX4 downstream targets, and E) a myogenic differentiation marker in cells at day 10 of differentiation. Relative expression was normalized to dC-Neg in each experimental set (n = 4). All RT-qPCR data are represented as mean ± SEM. \*P ≤ 0.05, \*\*P ≤ 0.01, \*\*\*P ≤ 0.001, \*\*\*\*P ≤ 0.0001, and ns indicates not significant as determined using one way ANOVA followed by the Tukey's multiple comparisons test. F) DNA methylation analysis of the D4Z4 regions using bisulfite sequencing. The identification numbers of sgRNAs are derived from the original work of Himeda et al<sup>31</sup>. Note that all the sgRNAs are located inside the D4Z4 unit but outside of the analyzed region.

Figure 2. A combination of dCas9-KRAB and dCas9-D3A/D3A3L slightly suppressed DUX4 with transient transfection. See also Figure S2.

659 A) Construct designs for the dCas9-effectors followed by internal ribosome entry site (IRES)-driven neomycin  
660 resistance marker for drug selection. B) Scheme showing the transfection, selection, and differentiation of iPSC  
661 clones to myocytes. FSHD2 iPSC<sup>tet-MyoD</sup> clones were transfected by electroporation with the dCas9-effector(Neo)  
662 and PBase together for constitutive expression, then for > 2 passages for the removal of PBase. Cells were transfected  
663 by electroporation with dCas9-effector(BFP) and sgRNAs together for transient expression. After two days, cells  
664 with BFP and RFP dual signals were sorted, expanded for two weeks, and differentiated for analysis. Note that the  
665 dCas9-effector is targeted only while sgRNAs are induced in cells, except for in condition 7 where PBase was added  
666 again in the second electroporation for constitutive expression of the sgRNAs. C) Experimental design for  
667 comparison. While dCas9-KRAB was expressed continuously, transient expression of the sgRNAs enabled the  
668 transient targeting of dCas9-effectors on the sites since PBase was excluded for 1-6. In addition, dCas9-KRAB(Neo)  
669 transfected with sgRNAs and PBase (7. cK) was also prepared as a positive control as its *DUX4* suppression effect  
670 was previously confirmed. D) RT-qPCR analysis for D) DUX4-fl, E) DUX4 downstream targets, and F) a myogenic  
671 differentiation marker in cells on day 10 of differentiation. Relative expression was normalized to condition.1 in each  
672 experimental set (n = 4). All RT-qPCR data are represented as mean ± SEM. \*P ≤ 0.05, \*\*P ≤ 0.01, \*\*\*P ≤ 0.001,  
673 \*\*\*\*P ≤ 0.0001, and ns indicates not significant as determined using one way ANOVA followed by the Tukey's  
674 multiple comparisons test.

675

676 Figure 3. Repeated transfection boosted silencing effect of transient combinations. See also Figure S3.

677 A) Scheme showing the transfection, selection, and differentiation of iPSC clones to myocytes. FSHD2 iPSC<sup>tet-MyoD</sup>

678 clones with constitutive dCas9-effector(Neo) were transfected by electroporation with dCas9-effector (BFP) and  
679 sgRNAs together for transient expression (the first transient electroporation). After two days, cells with BFP and RFP  
680 dual signals (tEP<sup>1</sup>) were sorted and expanded for two weeks followed by differentiation for analysis or for four days  
681 followed by a second round of transfection. Cells after the second round were sorted for BFP and RFP dual signals  
682 (tEP<sup>2</sup>) and expanded for two weeks followed by differentiation for analysis or for four days followed by a third round  
683 of transfection. Cells after the third round were sorted for BFP and RFP dual signals (tEP<sup>2</sup>) and expanded for two  
684 weeks followed by differentiation for analysis. Note that the dCas9-effector is targeted only while sgRNAs are  
685 induced in cells, except for condition 3, where PBase was added again in the second electroporation for constitutive  
686 expression of the sgRNAs. B) Experimental design for comparison. dCas9-KRAB(Neo) cells with one, two, and  
687 three rounds of sgRNAs and dCas9-D3A3L together (4-6. tEP1, tEP2 and tEP3). In addition, dCas9-NegNeo)  
688 transfected with sgRNAs as negative control (1. Neg) and dCas9-KRAB(Neo) transfected with sgRNAs without  
689 PBase (2. transient KRAB induction, tK) and with PBase as positive control (3. constitutive KRAB induction cK)  
690 were also prepared. C–E) RT-qPCR analysis for C) DUX4-fl, D) DUX4 downstream targets, and E) a myogenic  
691 differentiation marker in cells at day 10 of differentiation. Relative expression was normalized to the average for  
692 condition 1 in all samples. (n = 2–7). All data are represented as mean ± SEM. \*P ≤ 0.05, \*\*P ≤ 0.01, \*\*\*P ≤ 0.001,  
693 \*\*\*\*P ≤ 0.0001, and ns indicates not significant as determined using one way ANOVA followed by the Tukey's  
694 multiple comparisons test. F–G) Heatmaps showing the gene expression determined from the RNA-seq analysis of  
695 the differentiated Neg and tEP<sup>3</sup> cells from two independent experimental sets F) for the DUX4 associated gene set  
696 and G) the myogenic differentiation associated gene set. Exp.1 and Exp.2 indicate biologically independent

experimental sets. H) Volcano plot generated using the gene expression data from the RNA-seq analysis for all genes. Note that DUX4 target genes are significantly downregulated while most of genes are not significantly changed ( $-\log_{10}P \leq 5$ ). I) DNA methylation analysis for the D4Z4 regions determined by bisulfite sequencing. For the non-treated FSHD2 clone, the same data as in Figure 1F was used.

Figure 4. DUX4 could be suppressed by the transient activity of the dCas9-KRAB and dCas9-D3A3L combination in the FSHD1-iPSC model. See also Figure S4.

A) Scheme showing the transfection, selection, and differentiation of iPSC clones to myocytes. FSHD1 iPSC<sup>tet-MyoD</sup> clones were transfected by electroporation with a combination of dCas9-effector(Neo) and PBase for constitutive expression, then transfected by electroporation with both the dCas9-effector (BFP) and PBase for constitutive expression and sorted based on the BFP signal. After > 2 passages to remove the PBase after electroporation, cells were transfected by electroporation with sgRNAs together for transient expression and after two days sorted for BFP and RFP dual signals and expanded for 4 or 5 days. The transfection-sorting round was repeated three times followed by two weeks of expansion and differentiation for analysis. It is of note that the dCas9-effector is targeted only while sgRNAs are induced in cells, except for condition 3 where PBase was added again in the second electroporation for constitutive expression of sgRNAs. B) Experimental design for comparison analysis. Sample conditions were named as tNN (transient sgRNAs with dCas9-Neg(Neo) and dCas9-Neg(BFP)), tKN (transient sgRNAs with dCas9-KRAB(Neo) and dCas9-Neg(BFP)), cK (constitutive sgRNAs with dCas9-KRAB(Neo) and dCas9-Neg(BFP)), and tKD (transient sgRNAs with dCas9-KRAB(Neo) and dCas9-D3A3L(BFP)). C) Images of the phase and fluorescence



of RFP one week after the third round of transfection. Scale bar: 500  $\mu$ m. D–F) RT-qPCR analysis for D) DUX4-fl, E) DUX4 downstream targets, and F) a myogenic differentiation marker in cells at day 9 of differentiation. Relative expression was normalized to one sample from condition 1 [ $n = 3$ , except for condition tNN ( $n = 2$ )]. All data are represented as mean  $\pm$  SEM. \* $P \leq 0.05$ , \*\* $P \leq 0.01$ , \*\*\* $P \leq 0.001$ , \*\*\*\* $P \leq 0.0001$ , and ns indicates not significant as determined using one way ANOVA followed by the Tukey's multiple comparisons test.

Figure 5. Off-target analysis revealed the maximum potential off-target impact on global DNA methylation and the relevant minimum effect on the transcriptome. See also Figure S5.

A) Summary of sample conditions used in this analysis. tNN (with dCas9-Neg(Neo) and dCas9-Neg(BFP) constitutively introduced and sgRNAs transiently transfected three times) and tKD (with dCas9-KRAB(Neo) and dCas9-D3A3L(BFP) constitutively introduced and sgRNAs transiently transfected three times) of undifferentiated FSHD2 iPSC<sup>tet-MyoD</sup> from Figure S4 was used for the Infinium Methylation EPIC array. RNA-seq data from the Neg and tEP<sup>3</sup> of differentiated FSHD2 iPSC<sup>tet-MyoD</sup> (referred to conditions 1 and 6 in Figure 3C) were used. It is of note that tNN and tKD correspond to Neg and tEP<sup>3</sup>, respectively in this analysis. B) The plots of the averaged DNA methylation beta values for all filtered probes in the EPIC array among tKD and tNN ( $n = 2$  and 3, respectively). Significantly upregulated probes with a  $> 0.2$  increase in beta value and  $< 0.01$  BH adjusted p-value (up, shown in red) and downregulated probes with a  $> 0.2$  decrease in beta value and  $< 0.01$  BH adjusted p-value (down, shown in blue) on the y axis when compared to the x axis are emphasized, otherwise shown as not significant (ns, in gray). Dot lines show the borders for the cutoff with a 0.2 increase/decrease in beta value. C) Scheme showing the significantly

differential methylation based off-target evaluation. D) Summary of annotated gene numbers with certain numbers of significantly upregulated probes in 5B). Note that genes with more than three significantly upregulated relevant probes were defined as off-target gene candidates. E) Off-target gene candidates in Figure 5D were emphasized in red, otherwise in gray, in the RNA-seq data in Figure 3F–H. F) Scheme showing the *in silico* off-target prediction-based evaluation. See also supplementary Figure 5E for a detailed workflow of the *in silico* off-target prediction. G) Probes proximal to each predicted 8mer (in blue) and 12mer (in red) off-target binding site for all sgRNAs were emphasized in all dots of the averaged EPIC array beta value in tKD vs tNN (the same plots as Fig.5B). The lower table shows the percentages of dots in each definition. H) The annotated genes with at least one significantly upregulated probe ( $> 0.2$ ) from the off-target proximal probes in Fig.5G were merged using RNA-seq data in a similar way to 5E and relative changes were shown using a heatmap for each experimental set.

Figure 1

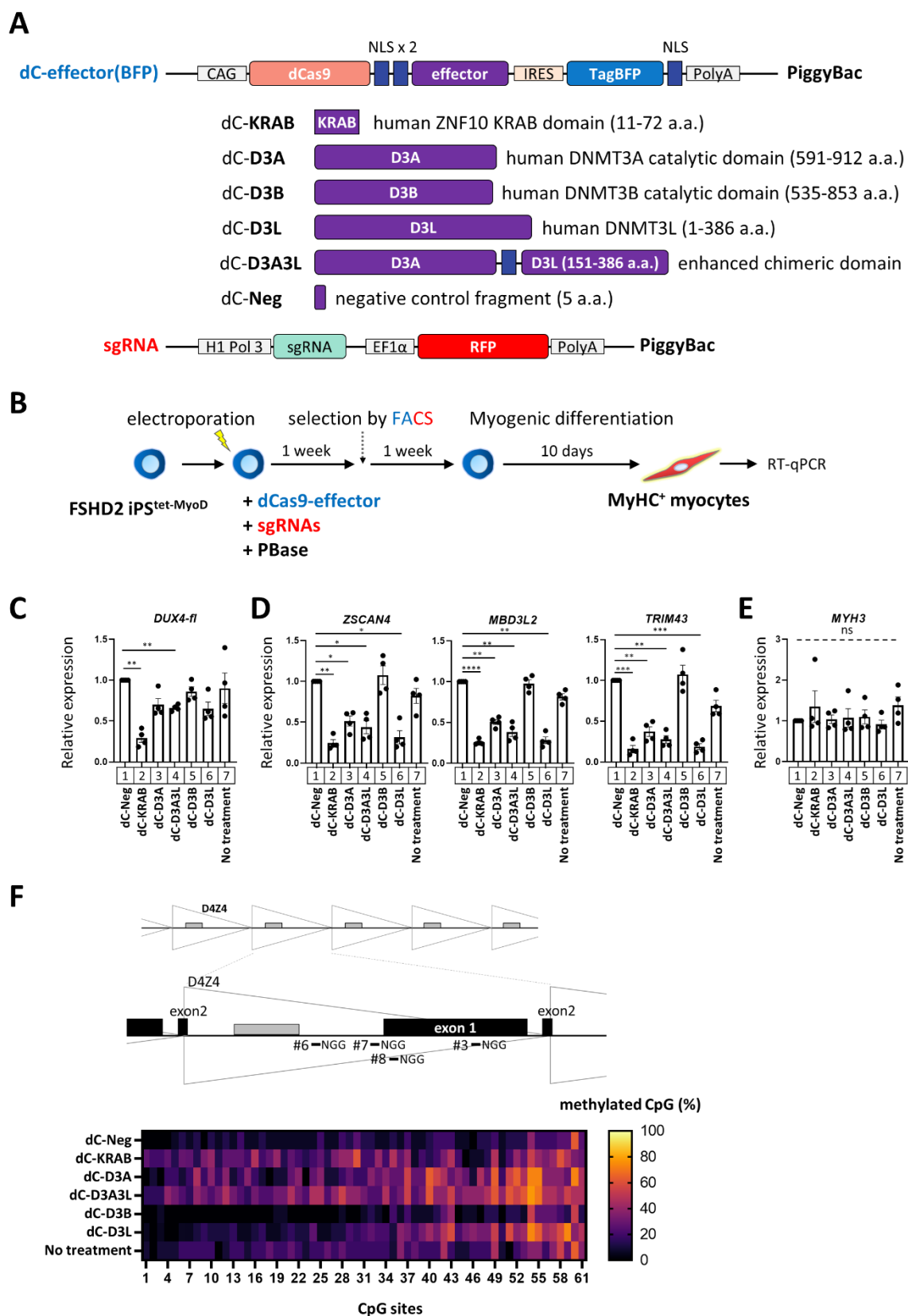


Figure 2

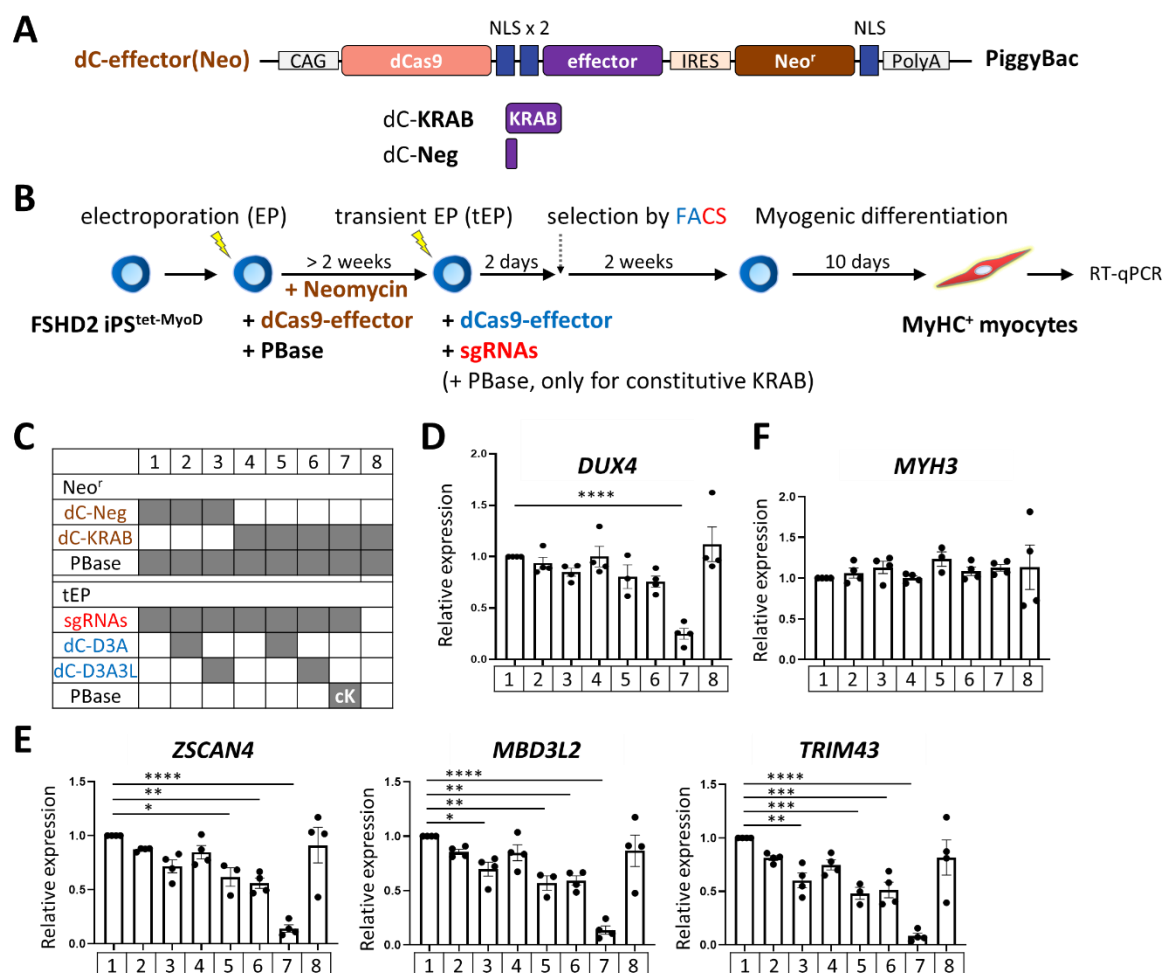


Figure 3

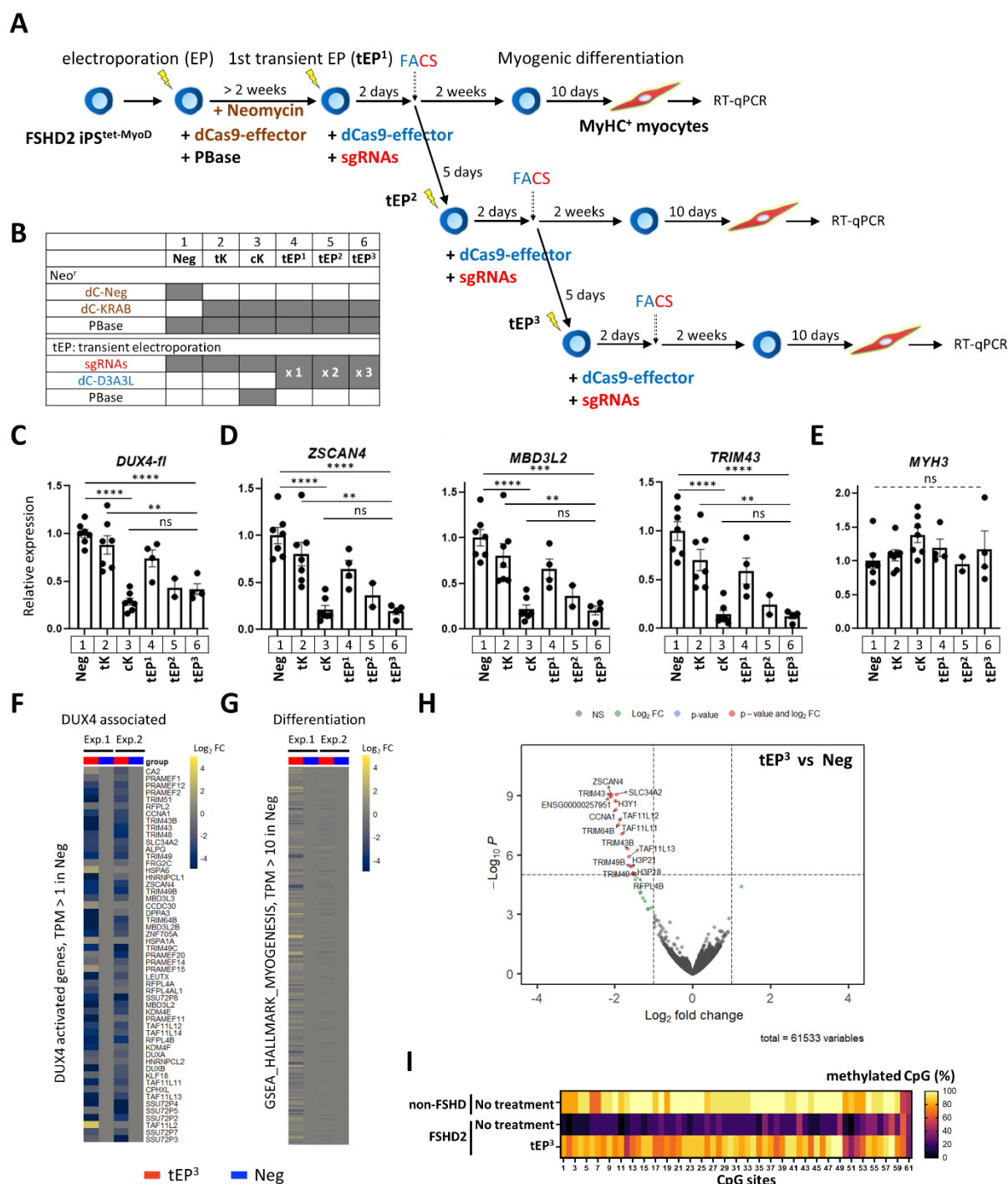


Figure 4

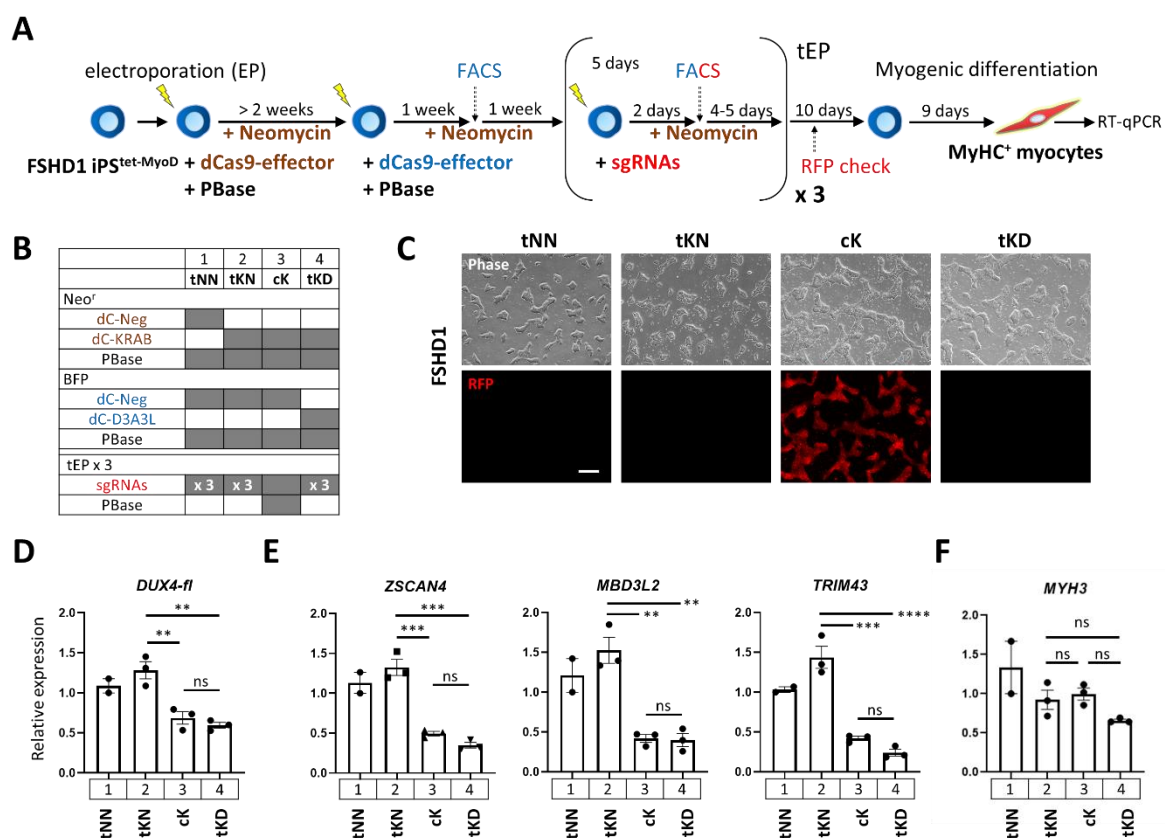
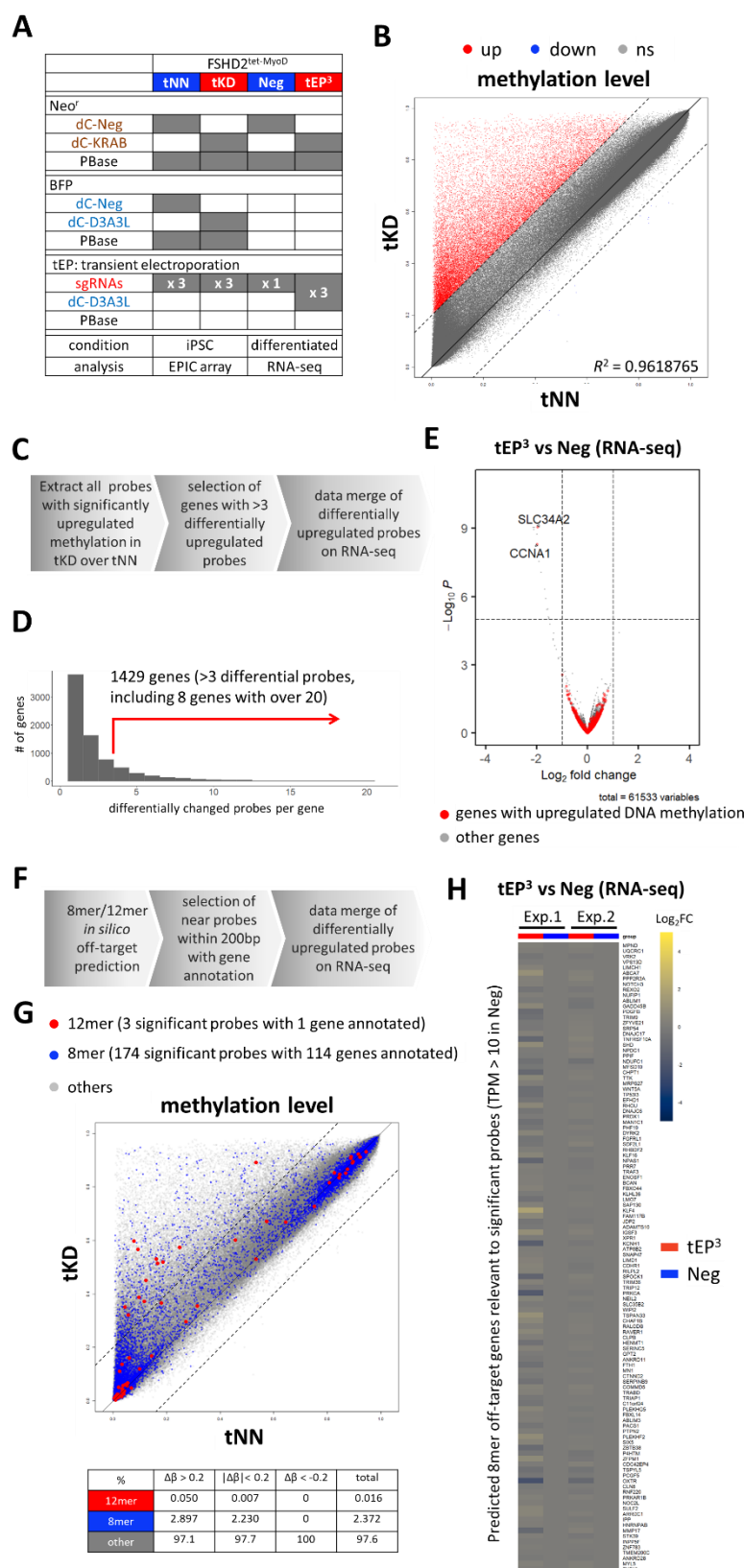


Figure 5



# Graphical abstract

